Nanotoxicology, May 2013; 7(3):235–250

ISSN: 1743-5390 print / 1743-5404 online
DOI: 10.3109/17435390.2011.649796

informa
healthcare

Effect of surface modification of silica nanoparticles on toxicity and cellular uptake by human peripheral blood lymphocytes *in vitro*

Anna Lankoff[1,2], Michal Arabski[1], Aneta Wegierek-Ciuk[1], Marcin Kruszewski[2,3], Halina Lisowska[1], Anna Banasik-Nowak[1], Krystyna Rozga-Wijas[4], Maria Wojewodzka[2] & Stanislaw Slomkowski[4]

[1]*Department of Radiobiology and Immunology, Institute of Biology, Jan Kochanowski University, Kielce, Poland,* [2]*Institute of Nuclear Chemistry and Technology, Centre for Radiobiology and Biological Dosimetry, Warsaw, Poland,* [3]*Institute of Agricultural Medicine, Lublin, Poland and* [4]*Centre of Molecular and Macromolecular Studies, Polish Academy of Sciences, Łódź, Poland*

Abstract

Silica nanoparticles have an interesting potential in drug delivery, gene therapy and molecular imaging due to the possibility of tailoring their surface reactivity that can be obtained by surface modification. Despite these potential benefits, there is concern that exposure of humans to certain types of silica nanomaterials may lead to significant adverse health effects. The motivation of this study was to determine the kinetics of cellular binding/uptake of the vinyl- and the aminopropyl/vinyl-modified silica nanoparticles into peripheral blood lymphocytes *in vitro,* to explore their genotoxic and cytotoxic properties and to compare the biological properties of modified silica nanoparticles with those of the unmodified ones. Size of nanoparticles determined by SEM varied from 10 to 50 nm. The average hydrodynamic diameter and zeta potential also varied from 176.7 nm (+18.16 mV) [aminopropyl/vinyl-modified] and 235.4 nm (−9.49 mV) [vinyl-modified] to 266.3 (−13.32 mV) [unmodified]. Surface-modified silica particles were internalized by lymphocytes with varying efficiency and expressed no cytotoxic nor genotoxic effects, as determined by various methods (cell viability, apoptosis/necrosis, oxidative DNA damage, chromosome aberrations). However, they affected the proliferation of the lymphocytes as indicated by a decrease in mitotic index value and cell cycle progression. In contrast, unmodified silica nanoparticles exhibited cytotoxic and genotoxic properties at high doses as well as interfered with cell cycle.

Keywords: Surface-modified silica nanoparticles, kinetics of cellular binding/uptake, oxidative DNA damage, chromosome aberrations, apoptosis, cell cycle analysis, human lymphocytes

Introduction

In the past few years, nanotechnology has shown great promise in a broad interdisciplinary area of research and industrial activity (Barik et al. 2008). The increased accessibility of nanomaterials has led to development of research focusing on application of nanomaterials in drug delivery, cancer therapeutics, gene therapy and molecular imaging. Among nanomaterials, silica nanoparticles have received considerable attention due to their unique properties. In particular, mesoporous silica nanoparticles exhibit several attractive features, including particle size control, relatively straightforward functionalization, degradability under physiological conditions and a large surface area and pore volume allowing the incorporation of large amounts of cargo if needed (Rosenholm et al. 2010). They exhibit multifunctional properties, simultaneously carrying fluorescent dyes for imaging, ligands for targeting of specific cells, cell-death-inducing photosensitizers, drugs and genes for therapy (Taylor et al. 2008; Chen et al. 2010; Cho et al. 2010). The potential applications of mesoporous silica as molecule carrier have been expanded into the biomedical field for bone tissue regeneration purposes (Vallet-Regi et al. 2007). Recently, a large amount of research has been devoted to the development of surface-modified mesoporous silica nanoparticles (reviewed by Knopp et al. 2009). The surface of silica nanoparticles can be functionalized by various organic/inorganic groups such as silanol, octadecyl, amine, carboxyl, polyethylene glycol, vinyl and other groups (Bagwe et al. 2006; An et al. 2007; Holmes et al. 2009; Hom et al. 2009; Di Pasqua et al. 2007). It was reported that such modified silica nanoparticles offer the potential of monitoring, repairing, constructing and controlling human biological systems at the molecular level (reviewed by Oberdörster et al. 2005). Despite these potential benefits, there is concern that exposure of humans to certain types of silica nanomaterials may lead to significant adverse health effects. Hence, there is increasing demand on development of modified silica nanoparticles of low or neglectable toxicity. This can be accomplished by modifying the surface of

Correspondence: Anna Lankoff, Department of Radiobiology and Immunology, Institute of Biology, Jan Kochanowski University, Swietokrzyska 15, 25-406 Kielce, Poland. Tel: +4841 349 62 98. Fax: +4841 349 62 92. E-mail: alankoff@gmail.com

(Received 4 January 2011; accepted 22 November 2011)

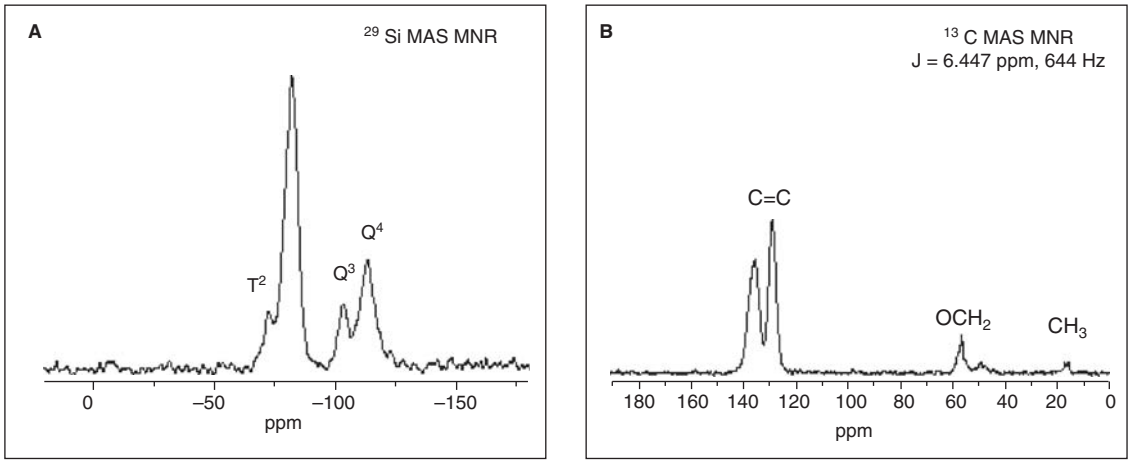

Figure 1. NMR spectra of the vinyl-modified silica nanoparticles obtained by hydrolytic polycondensation of mixture of TEOS and vinyltriethoxysilane in a base aqueous solution, using Pluronic F-68 as a surfactant [$ViSi(OEt)_3$: TEOS (1 :1)], $T^2 = (CH_2 = CH)Si(OH)(OSi)_2$; $T^3 = (CH2 = CH)Si(OSi)_3$; $Q^3 = (HO)Si(OSi)_3$; $Q^4 = Si(OSi)_4$. (A) ^{29} Si MAS NMR spectra of the silica nanoparticles, (B) ^{13} C MAS NMR spectra of the silica nanoparticles.

nanoparticles to make them more biocompatible. Therefore, we modified the surface of silica nanoparticles with vinyl or aminopropyl/vinyl groups that can be further utilized as linkers for attachment of biologically active macromolecules. In addition, to get insight into potential factors determining toxicity of silica nanoparticles, the objective of this study was: (1) to synthesize and characterize silica nanoparticles of the similar size, shape but differing in surface charge; (2) to determine their uptake kinetics into peripheral blood lymphocytes *in vitro*; (3) to explore the genotoxic and cytotoxic properties of these nanoparticles; and (4) to compare the biological properties of modified silica nanoparticles with those of the unmodified ones.

In spite of the numerous studies on the toxicity of silica nanoparticles in model *in vitro* systems, an increasing number of potential applications of silica nanoparticles in medicine raises question about its safety with regard to native human cells. The cell lines in culture are usually cancer or immortalized (virus transfected) cell lines that have different properties with respect to cellular signaling, apoptosis induction, DNA damage response and cell cycle progression than primary cells. Hence, we have chosen primary peripheral blood lymphocytes as an experimental *in vitro* model and employed various techniques: flow cytometry to monitor the kinetics of cellular binding/uptake of silica nanoparticles into lymphocytes and the cell cycle progression, the comet assay in conjunction with Fpg to determine ROS-induced DNA damage and the chromosome aberration assay to evaluate the clastogenic activity of the tested nanoparticles. The occurrence of apoptosis and necrosis was estimated by the annexin method.

Materials and methods

Tetraethoxysilane (TEOS; 99%), aminopropyltrimethoxysilane (APTES; 99%) and vinyltriethoxysilane (VTES; 98%) were reagent-grade products of Gelest and used without further purification. Ethanol and methanol from Polskie Odczynniki Chemiczne POCh, Poland (analytical grade), used as the solvent for sol-gel processes were purified according to standard methods described by Perrin et al. (1980). Poly (ethylene glycol)-*block*-poly (propylene glycol)-*block*-poly (ethylene glycol) triblock copolymer (Mavg. = 8400, Pluronic F−68) and sodium dodecyl sulfate (SDS; 99%) were purchased from Aldrich and used as received. Silica nanoparticles were purchased from Sigma-Aldrich [Cat. No: 637246].

Synthesis of functionalized silica nanoparticles

For preparation of the vinyl-modified silica nanoparticles a water suspension sol-gel process was used. The hydrolytic polycondensation of tetraethoxysilane (TEOS) and vinyltriethoxysilan mixture was performed at ambient temperature in a base aqueous solution using Pluronic F-68 as a surfactant (Rózga-Wijas et al. 2005). The aminopropyl/vinyl-modified silica particles were synthesized following the Stöber method in ethanol with APTES as catalyst and source of silica (Stöber et al. 1968; Green et al. 2003; Arkhireeva et al. 2003). Supplementary materials provide detailed information dealing with synthesis of nanoparticles.

Characterization of silica nanoparticles

Chemical analyses of silica nanoparticles for C, H and N were performed using a Euro EA elemental analyzer made by Euro Vector Instruments & Software. Thermogravimetric analysis (TGA) was performed with a Hi-Res TGA 2950 thermal analyzer. The TGA measurements were carried out in a nitrogen atmosphere at a heating rate of 10°C/min from 30 to 960°C. Nitrogen adsorption-desorption isotherms were determined using an ASAP 2010 Micromeritics Sorption Analyser. Samples were degassed for 6 h at 150°C under vacuum prior to analysis. The Brunauer-Emmett-Teller (BET) surface areas were evaluated using adsorption data in a relative pressure range from 0.05 to 0.9 and calculated by the BET method. The mesopore size distribution was calculated on the basis of adsorption branches using the Barrett-Joyner-Halenda (BJH) model. ^{13}C and ^{29}Si solid-state NMR studies were performed on a Brucker DSX 300 spectrometer with samples in 4-mm zirconia rotors. ^{13}C CP/MAS NMR spectra were obtained at 75.47 MHz using

Table I. Characteristics of surface composition of the unmodified silica nanoparticles, the vinyl-modified silica nanoparticles and the aminopropyl/vinyl-modified silica nanoparticles.

Nanoparticles	Functional group R	Elemental analysis (wt %C: wt %N) (a)	Content of R by elemental analysis [mmol/g]	Content of R by XPS analysis [mmol/g]	Elemental analysis teoret wt % (b)				wt % by XPS analysis (c)				^{29}Si(MAS) NMR relative peak area (mol % of total) (d)			TGA analysis (g)
					Si	C	O	N	Si	C	O	N	T (e)	Q (f)	T/Q	
Unmodified silica nanoparticles	-	wt %C <0.3	-	-	46.67	-	53.34	-	48.73	0.79	50.48	-	n.d.	n.d.	n.d.	n.d.
Vinyl-modified silica nanoparticles	-CH = CH2	wt %C 16.82	5.10	1.37 C2H3 3.06 C2H5	40.29	17.27	40.29	-	41.64	19.49	37.92	-	66.91	33.09	2.02	13.12% - 580°C 84.91% - res
Aminopropyl/ vinyl-modified silica nanoparticles	-CH = CH2 -(CH2)3NH2	wt %C 18.88 wt %N 3.41	2.43 4.10	1.39 C2H3 1.93 C3H4NH2	36.53	19.74	36.30	3.97	40.23	19.25	36.03	2.75	62.79	37.21	1.69	17.78% - 550°C 80.68% - res

(a) elemental analysis of carbon and nitrogen; (b) assumption that all CH2 CH2 OSi groups were hydrolyzed and condensed; (c) wt % on surface; (d) nuclear magnetic resonance spectroscopy (NMR) analysis; (e) T = (SiO)3-n(OH)n Si-C, n = 0, 1, 2; (f) Q = (SiO)4-n(OH)n Si, n = 0, 1; (g) thermogravimetric analysis; n.d, not determined.

cross polarization (CP) and magic angle spinning (MAS) at a rate of 8 kHz, applying 90° pulse and 6.0 s pulse delays. ^{29}Si CP/MAS NMR spectra were recorded at 59.63 MHz, applying 90° pulses, 6 s pulse delays and 3 ms contact time, with samples in 4.0-mm zirconia rotors at a rate of 8 kHz. The hydrodynamic diameter of silica nanoparticles was measured by dynamic light scattering (DLS). DLS was performed at 25°C with a scattering angle of 90° on the Zeta-sizer Nano ZS (Malvern, Malvern Hills, UK). Stock solutions of nanoparticles were diluted 1:4 in RPMI 1640 cell culture medium and measured in triplicate with 20 sub-runs. Scanning electron microscope (SEM) analyses were performed using DSM 942 microscopy (Zeiss, Germany) in the secondary electron (SE) mode. SEM worked with parameters: high voltage EHT 2 kV, working distance (WD) = from 4 to 4.8 mm. Surfaces of samples were sputter-coated with carbon. Zeta potential of nanoparticles in RPMI 1640 cell culture medium (pH 7.4) was measured using Zetasizer 3000 HS Malvern Instruments. The surface chemistry of silica nanoparticles was analyzed by X-ray photoelectron spectroscopy (XPS). Supplementary materials provide detailed information dealing with XPS analyses and results.

Dispersion of silica nanoparticles

Silica nanoparticle stock solutions were prepared by dispersion of 2 mg of nanoparticles in 800 µl of distilled water. Nanoparticle dispersions were sonicated on ice using a probe sonicator (Bronson, USA) with 420 J/m^3 total ultrasound energy. Bovine serum albumin (100 µl) 15% and 100 µl of a 10 x concentrated PBS were given immediately after sonication. Stock solutions were prepared before each experiment.

Limulus amebocyte lysate (PyroGene rFC) assay

Endotoxin level in nanoparticle stock solutions was determined by the fluorogenic endotoxin detection assay PyroGene rFC purchased from Lonza (Walkersville, USA). The PyroGene test utilizes recombinant Factor C (rFC), which is used in combination with a fluorogenic substrate. rFC is more selectively an endotoxin-sensitive factor as proteins used in chromogenic LAL assay. rFC recognizes only endotoxin without glucans in contrast to LAL assay. The reaction mixtures contained nanoparticles at concentrations of 1–100 µg/ml. All procedures were done in accordance with the test instruction.

Cell culture

Human venous blood was collected from three healthy donors (in two repetitions) into heparinized (10–20 U/ml) Greiner bio-one tubes. Peripheral blood mononuclear cells were isolated by Histopaque-1077 density gradient centrifugation, washed two times with phosphate buffered saline (PBS) and centrifuged at 900 x g for 10 min. The pellet containing lymphocytes was suspended at a density of 5 × 10^5 cells/ml in RPMI 1640 medium supplemented with 20% fetal bovine serum, 10 µg/ml PHA (phytohemagglutinin), 2 mM L-glutamine, 100 U/ml penicillin and 100 µg/ml streptomycin. The cultures were incubated at 37°C and 5% CO_2.

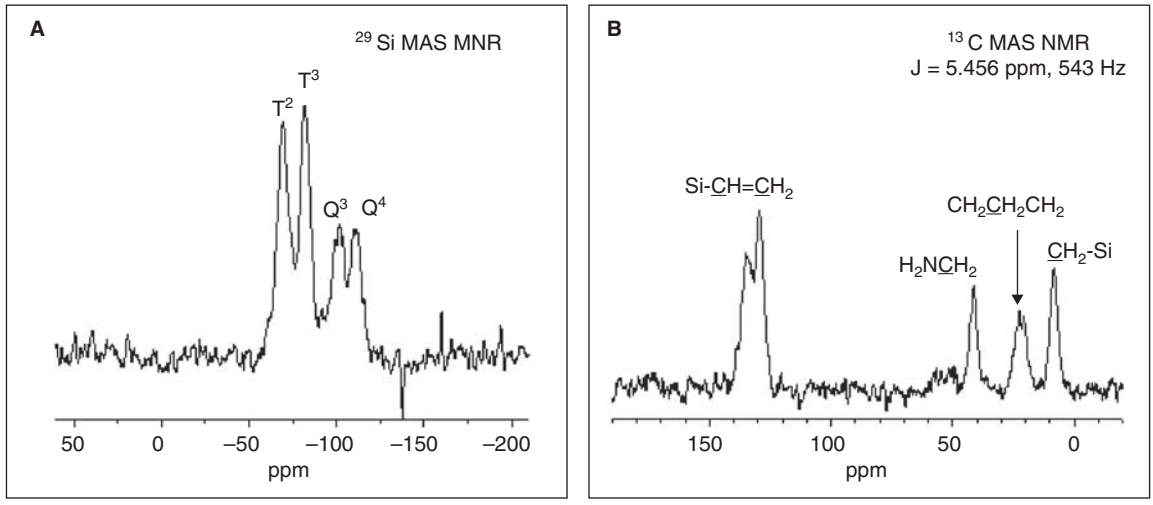

Figure 2. NMR spectra of the aminopropyl/vinyl- modified silica nanoparticles synthesized by the Stöber method. Density of ($H_2NCH_2CH_2CH_2$-) group 2.43 mol x g^{-1}, T^2 = C-Si(OH)$(OSi)_2$; T^3 = C-Si$(OSi)_3$; Q^3 = (HO)Si $(OSi)_3$; Q^4 = Si$(OSi)_4$. (A) ^{29} Si MAS NMR spectra of the silica nanoparticles, (B) ^{13} C MAS NMR spectra of the silica nanoparticles.

Kinetics of cellular binding/uptake of silica nanoparticles into human peripheral blood lymphocytes *in vitro*

The kinetics of cellular binding/uptake of silica nanoparticles into human peripheral blood lymphocytes *in vitro* was examined by analyzing forward scatter (FSC) versus side scatter (SSC) using flow cytometry (Becton Dickinson, LSR II flow cytometer containing a 488-nm laser, FSC diode detector and photomultiplier tube SSC detector) as described by Suzuki et al. (2007) and Zucker et al. (2010). SSC distribution ratio was chosen as a measure of cellular binding/uptake and was calculated by dividing the SSC value in the nanoparticle-treated cells by the SSC value in the nanoparticle-free cells. Two sets of experiments were performed. In the first experiment, human peripheral blood lymphocytes were treated with 10, 25, 50 and 100 μg/ml of unmodified silica nanoparticles for 1–6 h. In the second experiment, human peripheral blood lymphocytes were treated with 100 μg/ml of vinyl-modified, aminopropyl/vinyl-modified silica nanoparticles and unmodified silica nanoparticles for 1–24 h. After treatment with nanoparticles, cells were washed three times with PBS to ensure particle removal from the outer cell membrane. After centrifugation, cells were resuspended in 1 ml PBS for flow cytometry. Following gating, control and nanoparticle-exposed cells were run and plotted to examine the increase in SSC. Data for 50,000 events were stored per point. Because the flow rate affects these measurements, they were always performed at low flow rates. The cytometer was set up to measure SSC logarithmically and FSC linearly.

Analysis of cell viability, apoptosis and necrosis

Peripheral blood lymphocytes were treated with 10, 25, 50, 100 and 200 μg/ml of vinyl-modified, aminopropyl/vinyl-modified silica nanoparticles and unmodified silica nanoparticles for 2 and 24 h. As a positive control, lymphocytes were exposed to 12 μM camptothecin for 4 h. The frequencies of viable, apoptotic and necrotic cells were detected with the Annexin V-FITC apoptosis detection Kit I (BD Pharmingen, USA), according to Darzynkiewicz (2003). Briefly, cells were washed two times with cold PBS and then resuspended in a 1 X binding buffer at a concentration of 1×10^6 cells/ml. Cell suspension (100 μl) was incubated with 5 μl of Annexin V-FITC and 5 μl of PI (propidium iodide) at room temperature for 15 min in the dark. The cells were resuspended in 400 μl of a 1 x binding buffer. The fluorescence was determined using a LSR II flow cytometer (Becton Dickinson). A computer system BD FACSDiVa (version 6.0, Becton Dickinson) was used for data acquisition and analysis. Data for 20,000 events were stored. A cell gate containing human peripheral blood lymphocytes was established on the basis of the forward and side light scatters. Four different populations of cells are detected with the Annexin V-FITC kit: viable cells that are annexin negative and PI negative and express no fluorescence, early apoptotic cells that are annexin positive and PI negative and that express green fluorescence, late apoptotic/necrotic cells that are annexin positive and PI positive and that express green and orange fluorescence, necrotic cells that are annexin negative and PI positive and that express orange fluorescence.

Analysis of DNA damage

Human peripheral blood lymphocytes were treated with 10, 25, 50 and 100 μg/ml of vinyl-modified, aminopropyl/vinyl-modified silica nanoparticles and unmodified silica nanoparticles for 2 and 24 h. After treatment, the cells were washed twice with PBS, trypsynized and the alkaline comet assay was performed according to Wojewodzka et al. (1998). In brief, 200 μl of cell suspension containing about 100,000 cells was mixed with 200 μl of 2% low melting temperature agarose at 37°C and then placed on a slide pre-coated with a dried thin layer of 0.5% normal melting agarose. The cell suspension was covered with a coverglass and the slides were kept at 4°C for 5 min to allow solidification of the agarose. After removing the coverglass, the cells were lysed in a lysing solution (2.5 M NaCl, 100 mM EDTA, 10 mM Tris (tris(hydroxymethyl)aminomethane), 1% Triton X-100, pH 10) for 1 h. After washing in twice-distilled water

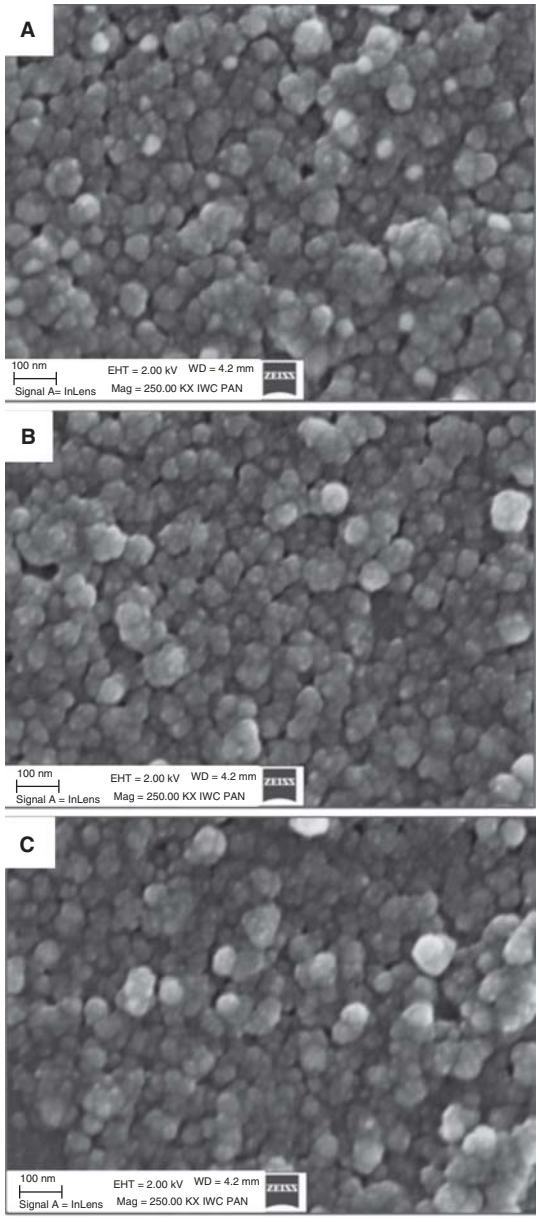

Figure 3. SEM micrographs of silica nanoparticles with particle size at the nanometer scale. (A) SEM micrograph of unmodified silica nanoparticles, (B) SEM micrograph of the vinyl modified nanoparticles (C) SEM micrograph of the aminopropyl/vinyl-modified nanoparticles.

the slides were placed on a horizontal gel electrophoresis chamber. The chamber was filled with electrophoretic buffer (1 mM EDTA, 300 mM NaOH, pH 13) and slides were kept in this buffer at 4°C for 20 min to allow the DNA to unwind. Electrophoresis was performed for 20 min (0.9 V/cm, 300 mA). After electrophoresis, the slides were washed three times with a neutralization buffer (0.4 M Tris, pH 7.5). All preparative steps were conducted in the dark to prevent additional DNA damage. The slides were stained with 1 μM DAPI (diamino-2-phenyl-indol) for 24 h and scored with Comet Analysis Software (Metasystems, Germany). The images were captured using Zeiss Axioplan 2 imaging fluorescence microscope (Carl Zeiss, Germany) equipped with triple band filter. A total of 200 cells per sample were randomly selected and analyzed. The extent of DNA damage

Table II. Summary of the vinyl-modified, aminopropyl/vinyl-modified and unmodified silica nanoparticle characteristics.

Nanoparticles	Size [nm] (a)	Hydrodynamic diameter [nm] (b)	Zeta potential [mV] (c)	BET surface area [m^2/g]	Total pore volume [cm^3/g]	Micropore volume [cm^3/g]	Average pore diameter [nm] by BET	BJH desorp.aver. pore diameter [nm]
Unmodified silica nanoparticles	10–50	266.3 ± 7.2	−13.32	640	n.d.	n.d.	n.d.	n.d.
Vinyl-modified silica nanoparticles	10–50	235.4 ± 4.9	−9.49	350	0.63	0.03	7.32	25.20
Aminopropyl/vinyl-modified silica nanoparticles	10–50	176.7 ± 5.1	+18.16	260	1.13	0.00	17.36	17.41

(a) nanoparticle size determined by SEM [nm]; (b) hydrodynamic diameter determined by photon correlation spectroscopy (DLS method); (c) zeta potential [mV] determined at 1.63×10^{-1} mol/kg and the pH 7.4 (in RPMI 1640 medium) during measurements of zeta potentials; n.d., not determined.

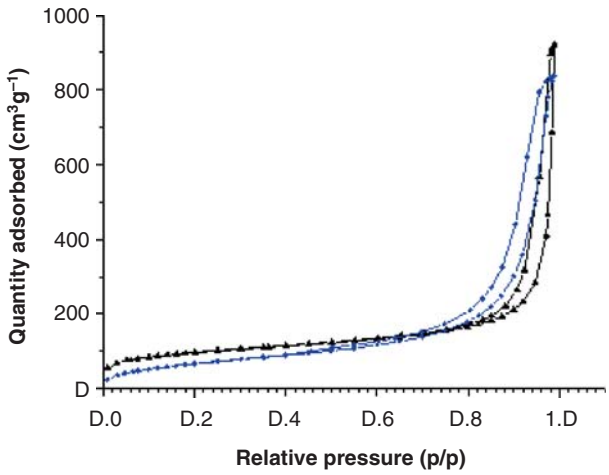

Figure 4. Nitrogen adsorption-desorption isotherm plots of the vinyl-modified silica nanoparticles (-▲-) and the aminopropyl/vinyl-modified nanoparticles (-●-).

was expressed as the percentage DNA in the comet tail (Collins 2004). To determine the level of oxidized bases, the modified comet assay was performed, using the purified oxidative DNA damage-specific enzyme Fpg (formamidopyrymidine DNA glycosylase, which catalyzes the excision of oxidized purines) (Kruszewski (1998). All preparative steps were conducted according to the protocol described earlier, with additional steps: after the lysis the slides were washed three times for 5 min with endonuclease buffer (0.1 M KCl, 0.5 mM EDTA 40 mM HEPES-KOH (4-(2-hydroxyethyl)-1-piperazineethanesulfonic acid), 0.2 mg/ml bovine serum albumin, pH 8.0). A 50-µl aliquot of Fpg was added; it was then covered with a coverglass and incubated at 37°C for 30 min. In parallel the control slides were incubated with endonuclease buffer at 37°C for 30 min. The slides were then processed as described earlier.

Analysis of chromosome aberrations and mitotic indices

Human peripheral blood lymphocytes were treated with 10, 25, 50 and 100 µg/ml of vinyl-modified, aminopropyl/vinyl-modified silica nanoparticles and unmodified silica nanoparticles. As a positive control, lymphocytes were exposed to a 2-Gy dose of X-rays (dose rate 1,13 Gy/min, 200 kV, 4,5 mA, YXLON Smart 200, Denmark). Bromodeoxyuridine (BrdU) (10 µM final concentration) was added to each experimental group to allow identification of the first division metaphases. Lymphocytes were placed in the incubator (37°C and 5% $C0_2$) and cultured for 50 h. Colcemid (0.15 µg/ml) was added for the final 2 h. Cells were harvested by the standard cytogenetic technique (Lankoff et al. 2003), dried and stained by the FPG (Fluorescence-plus-Giemsa) method (Perry & Wolf 1974). Mitotic indices (MI) were calculated by counting 1000 cells per point. The analysis of chromosome aberrations was performed on a minimum of 100 metaphase cells per point. Structural chromosome aberrations: chromatid-type and chromosome-type acentric fragments, dicentrics and ring chromosomes were determined according to Savage (1975) and were presented as mean value ± SD per cell from three independent experiments.

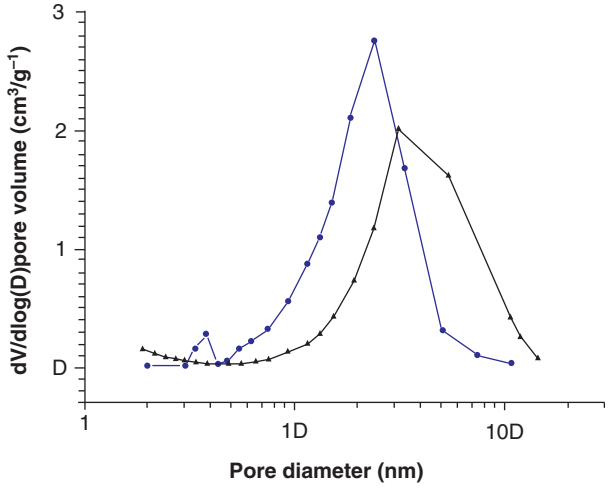

Figure 5. Pore size distribution plots of the vinyl-modified silica nanoparticles (-▲-) and the aminopropyl/vinyl-modified nanoparticles (-●-).

Flow cytometric analysis of the cell cycle

The sample preparation was performed as previously reported (Krishan 1975). Briefly, human peripheral blood lymphocytes were incubated in PHA containing culture medium with surface-modified and unmodified silica nanoparticles for 50 h. The cells were washed once with PBS and fixed at 4°C with 1 ml cold 70% ethanol for ≥ 30 min. Ethanol was removed by centrifugation at 2000 rpm for 5 min and PBS was added to wash the pellets. The cellular DNA was stained with propidium iodide (PI) solution (50 mg/ml, 0.1% Triton X-100, 0.1 mmol/L EDTA and 50 mg/ml RNase A in PBS) for 30 min at room temperature and stored at 4°C until measurement. DNA flow cytometry was performed on a LSR II flow cytometer (Becton Dickinson). A computer system BD FACSDiVa (version 6.0, Becton Dickinson) was used for data acquisition and Modfit LT (Verity) software was used for data analysis.

Statistical analysis

Statistical analysis of the obtained data was performed using Statistica 7.1 software (Stat Soft. Inc., Tulsa, USA). Data were evaluated by Kruskal-Wallis One Way Analysis of Variance on Ranks (ANOVA) followed by Dunnet's method (results of flow cytometry) and by ANOVA followed by Mann-Whitney Rank Sum test (all other data). Differences were considered statistically significant when the p value was ≤0.05.

Results

Synthesis and characterization of functionalized silica nanoparticles

The sol-gel polycondensation process and the Stöber method allowed us to obtain the vinyl-modified and aminopropyl/vinyl-modified silica nanoparticles with high yield. The vinyl-modified silica nanoparticles contained small amount (9.66 mol %) of Q^3 siloxane units, in which silicon was bonded to one OR (R = Et or H) group. This is

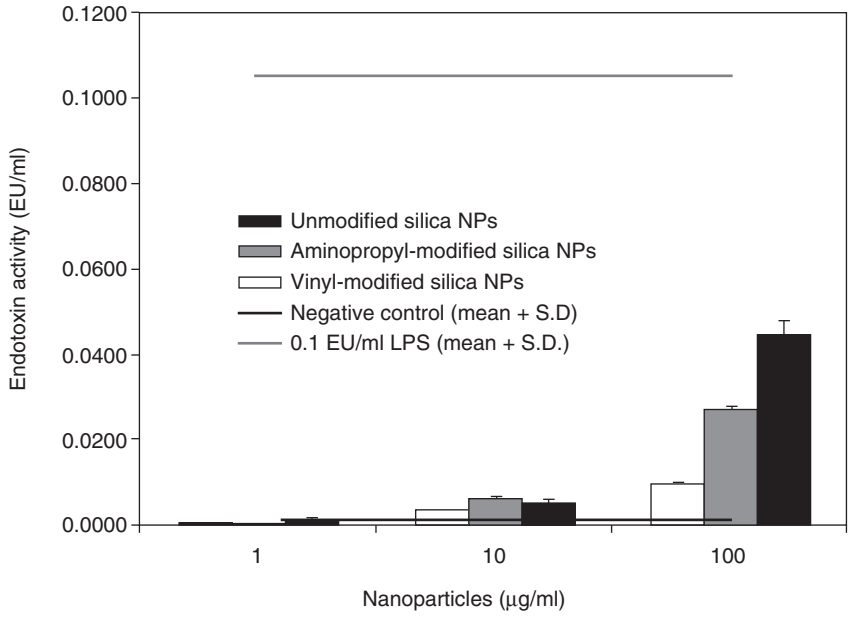

Figure 6. Endotoxin level in silica nanoparticle solutions (EU/ml). Three concentrations of unmodified, vinyl- and aminopropyl -modified silica nanoparticles were tested (1, 10, 100 μg/ml). Commercially available endotoxin standard and LAL water were used as positive and negative controls, respectively. Data are expressed as means ± S.D. from three independent experiments.

demonstrated by ^{29}Si CP/MAS NMR spectrum (Figure 1A, Table I). The complete removal of surfactants from vinyl-modified silica particles was observed by the ^{13}C MAS NMR analysis (Figure 1B) and by the GPC analysis of concentrated THF extract of the purified nanosilica (data not shown). Somewhat more Q^3 units (19.62 mol %) were found in the aminopropyl/vinyl-modified silica nanoparticles (Figure 2A; Table I). Peaks characteristic of fully condensed T^3 = C-Si (OSi)3 species found at −81.94 ppm for vinyl-modified (56.8 mol %) and at −82.19 ppm for aminoprophyl- and vinyl-modified silica nanoparticles (33.3 mol %) are abundant. The less intense peaks observed at 72.51 ppm for vinyl-modified and at -69.84 ppm for aminopropyl/vinyl-modified particles can be assigned to T^2 = C-Si(OH)(OSi)2 species. The formation of T^1 and T^0 species is insignificant, suggesting that although the condensation is not fully completed, an unreacted, organically modified precursor is not present. It can be seen that the ^{13}C MAS NMR spectrum of aminopropyl/vinyl-modified particles exhibits intense carbon resonances characteristic of the corresponding organic groups (Figure 2B). X-ray photoelectron spectroscopy studies of silica nanomaterials confirmed the successful grafting of vinyl and aminopropyl groups onto the silica surface (Table I, Supplementary Table I, Supplementary Table II, Supplementary Figure S1 and Supplementary Figure S2). The XPS analysis of the aminopropyl/vinyl-modified silica nanoparticle surface showed the presence of silicon (40.23%), oxygene (36.03%), carbon (19.25%) and nitrogen (2.75%). The XPS analysis of the vinyl-modified silica nanoparticle surface showed the presence of silicon (41.64%), oxygene (37.92%) and carbon (19.49%). The XPS analysis of the unmodified silica nanoparticle surface showed the presence of silicon (48.73%), oxygene (50.48%) and a minimal presence of carbon (0.79%), which might be due to the incomplete hydrolysis of the alkoxide precursor used for their synthesis. Silica nanoparticles examined by SEM showed spherical morphology and the presence of agglomerates (Figure 3). The average diameters of vinyl-modified, aminopropyl/vinyl-modified silica nanoparticles and unmodified silica nanoparticles determined by SEM were in the range from 10 to 50 nm. The average hydrodynamic diameters of vinyl-modified, aminopropyl/vinyl-modified and unmodified silica nanoparticles estimated by DLS method were 235.4 ± 4.6, 176.7 ± 5.1 and 256.3 ± 7.2, respectively (Table II). The average zeta potential in pH 7.4 varied from +18.16 mV (aminopropyl/vinyl-modified), −9.49 mV (vinyl-modified) and −13.32 mV (unmodified) (Table II). The results of the sorption studies, presented

Table III. Endotoxin level in silica nanoparticle solutions (EU/ml). Three concentrations of unmodified, vinyl-modified and aminopropyl/vinyl-modified silica nanoparticles were tested (1, 10, 100 μg/ml). Commercially available endotoxin standard and LAL water were used as positive and negative controls, respectively.

Experimental groups	Dose [μg/ml]	EU/ml [mean ± SD]
Unmodified silica nanoparticles	1	0.0007 ± 0.0002
	10	0.0034 ± 0.0001
	100	0.0094 ± 0.0006
Vinyl-modified silica nanoparticles	1	0.0006 ± 0.0009
	10	0.0050 ± 0.0013
	100	0.0443 ± 0.0038
Aminopropyl/vinyl-modified silica nanoparticles	1	0.0004 ± 0.0004
	10	0.0058 ± 0.0006
	100	0.0269 ± 0.0011
Negative control	LAL water	0.0005 ± 0.0002
Positive control (LPS)	0,1 EU/ml	0.1000 ± 0.0054
RPMI 1640 medium (Sigma-Aldrich)	*	≤1.0000

Data are expressed as means ± S.D. from three independent experiments; *According to manufacturer's specification.

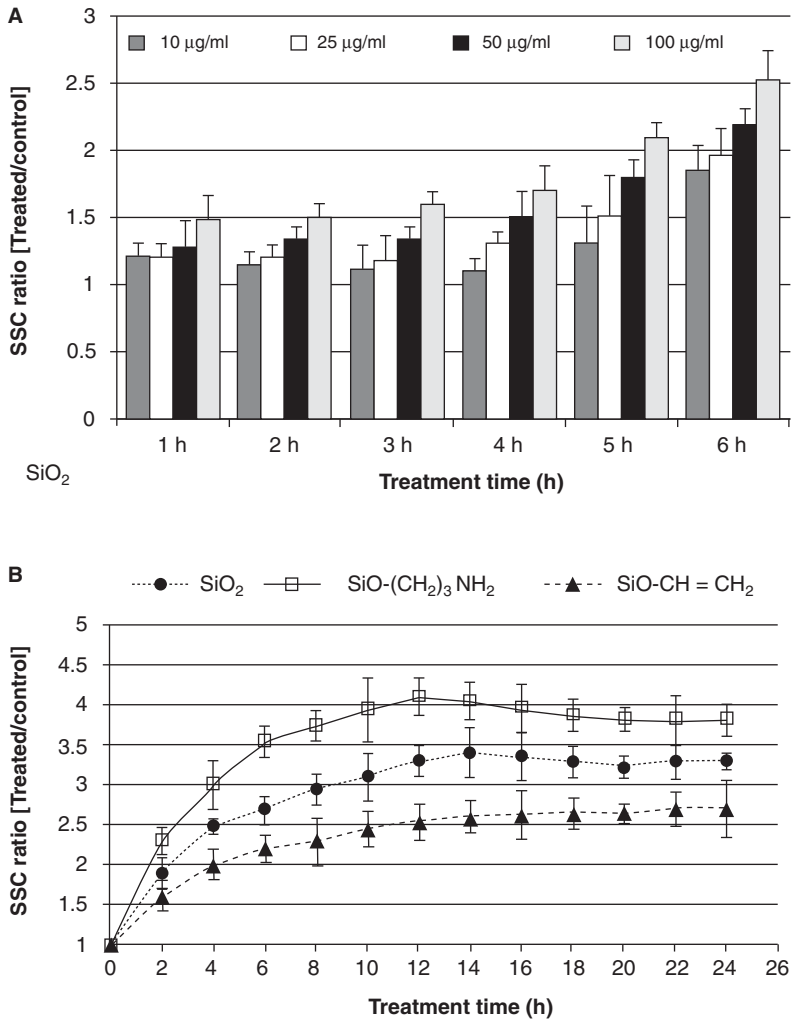

Figure 7. Cellular binding/uptake of silica nanoparticles into human peripheral blood lymphocytes *in vitro*. (A) relative changes in SSC versus the dose of unmodified silica nanoparticles and treatment time. Cellular binding/uptake was determined in lymphocytes treated with 10, 25, 50 and 100 μg/ml from 1 to 6 h. (B) relative changes in SSC versus treatment time. Cellular uptake was determined in lymphocytes treated with 100 μg/ml of unmodified (SiO_2), vinyl-modified ($SiO\text{-}CH = CH_2$) and aminopropyl/vinyl-modified ($SiO\text{-}(CH_2)3NH_2$) silica nanoparticles from 1 to 24 h. Data are expressed as means ± S.D. from three independent experiments.

in Table II, revealed that the average surface area values for vinyl-modified, aminopropyl/vinyl-modified and unmodified silica particles were 350 m^2/g, 260 m^2/g and 640 m^2/g, respectively. However, total volume of pores for vinyl-modified and aminopropyl/vinyl-modified particles were 0.63 cm^3/g and 1.13 cm^3/g, respectively (Figure 4). The adsorption-desorption isotherms exhibited by these materials are fairly typical of mesoporous solids with pore diameters in the range of 2–50 nm (type IV isotherm) (Figure 5). In both cases, the pore diameter distribution is broad (8–100 nm). The shape of these isotherms also is very close to that of a type II isotherm characteristic of macroporous solids. The isotherms display type H1 hysteresis, which is characteristic of solids made by aggregates or agglomerates of spherical particles of uniform size and shape, consistent with the results obtained using SEM. The thermal stability of the organic functional groups was determined by thermogravimetric analysis (Table I). After initial loss of solvent, the removal of the vinyl groups commenced at 340°C and continued up to 680°C (13.04 wt % of volatile products). Elimination of the aminopropyl and vinyl groups (17.78 wt %) takes place at the same conditions as earlier. An additional weight loss occurred at higher temperatures due to further condensation of the silicate walls, as observed in other mesoporous silicates.

The endotoxin level in nanoparticle stock solutions

Figure 6 and Table III present PyroGene test results with nanoparticle stock solutions at concentration of 1–100 μg/ml. The highest detected level of endotoxins in nanoparticle stock solution at concentration 100 μg/ml (0.04 EU/ml) was not higher than an acceptable level measured by the manufacturer (Sigma Aldrich) in RPMI 1640 medium (<1 EU/ml) used in all *in vitro* experiments.

Kinetics of cellular binding/uptake of silica nanoparticles into human peripheral blood lymphocytes *in vitro*

The first set of experiments was performed to get a perspective on the magnitude of the changing SSC and to choose the optimal dose of nanoparticles for the time-course experiments. The cells were exposed to 10, 25, 50 and 100 μg/ml silica nanoparticles from 1 to 6 h.

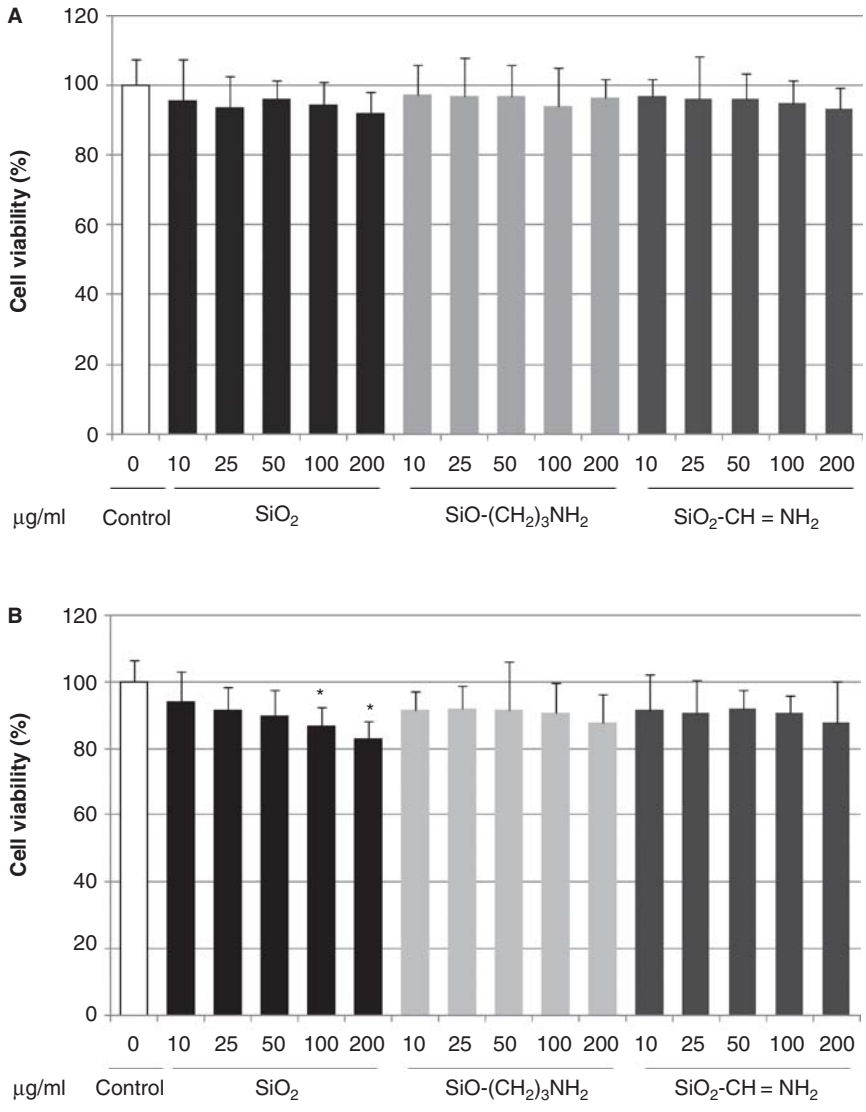

Figure 8. Flow cytometric analysis of cell viability of human peripheral blood lymphocytes *in vitro*, exposed to increasing doses of unmodified (SiO_2), vinyl-modified ($SiO-CH = CH_2$) and aminopropyl/vinyl-modified ($SiO-(CH_2)3NH_2$) silica nanoparticles for 2 and 24 h. (A) Cell viability of human peripheral blood lymphocytes exposed to 10, 25, 50, 100 and 200 μg/ml of silica nanoparticles for 2 h. (B) Cell viability of human peripheral blood lymphocytes exposed to 10, 25, 50, 100 and 200 μg/ml of silica nanoparticles for 24 h. Data are expressed as means ± S.D. from three independent experiments. Significant difference versus control, $*p < 0.05$.

As shown in Figure 7A, the SSC ratio increased in a dose- and time-dependent manner. A maximal increase in SSC ratio was observed in cells treated with silica nanoparticles at 100 μg/ml for 6 h (2.5-fold increase). This concentration was chosen for the time-course experiments. Peripheral blood lymphocytes were treated with 100 μg/ml of vinyl-modified, aminopropyl/vinyl-modified silica nanoparticles and unmodified silica nanoparticles for 1–24 h. Figure 7B presents differences in uptake profiles related to the type of nanoparticles at the same concentration values. It was observed that the uptake of all three types of nanoparticles was time-dependent. The uptake of nanoparticles increased gradually and reached a plateau at 12–14 h, depending on the type of nanoparticles. The uptake of aminopropyl/vinyl-modified silica nanoparticles by lymphocytes was more efficient than the uptake of silica and vinyl-modified nanoparticles.

The effect of silica nanoparticles on cell viability

Cell viability was determined in peripheral blood lymphocytes treated with 10, 25, 50, 100 and 200 μg/ml of vinyl-modified, aminopropyl/vinyl-modified silica nanoparticles and unmodified silica nanoparticles for 2 and 24 h. The results showed that there were no significant differences in the frequencies of viable cells between untreated cells and cells treated with modified silica nanoparticles for 2 and 24 h (Figure 8A, B). However, the frequency of viable cells was significantly decreased in lymphocytes treated with 100 and 200 μg/ml of unmodified silica nanoparticles for 24 h (Figure 8B).

The effect of silica nanoparticles on apoptosis and necrosis

As shown in Figure 9A and 9B, there were no significant differences in the frequencies of early apoptotic and late

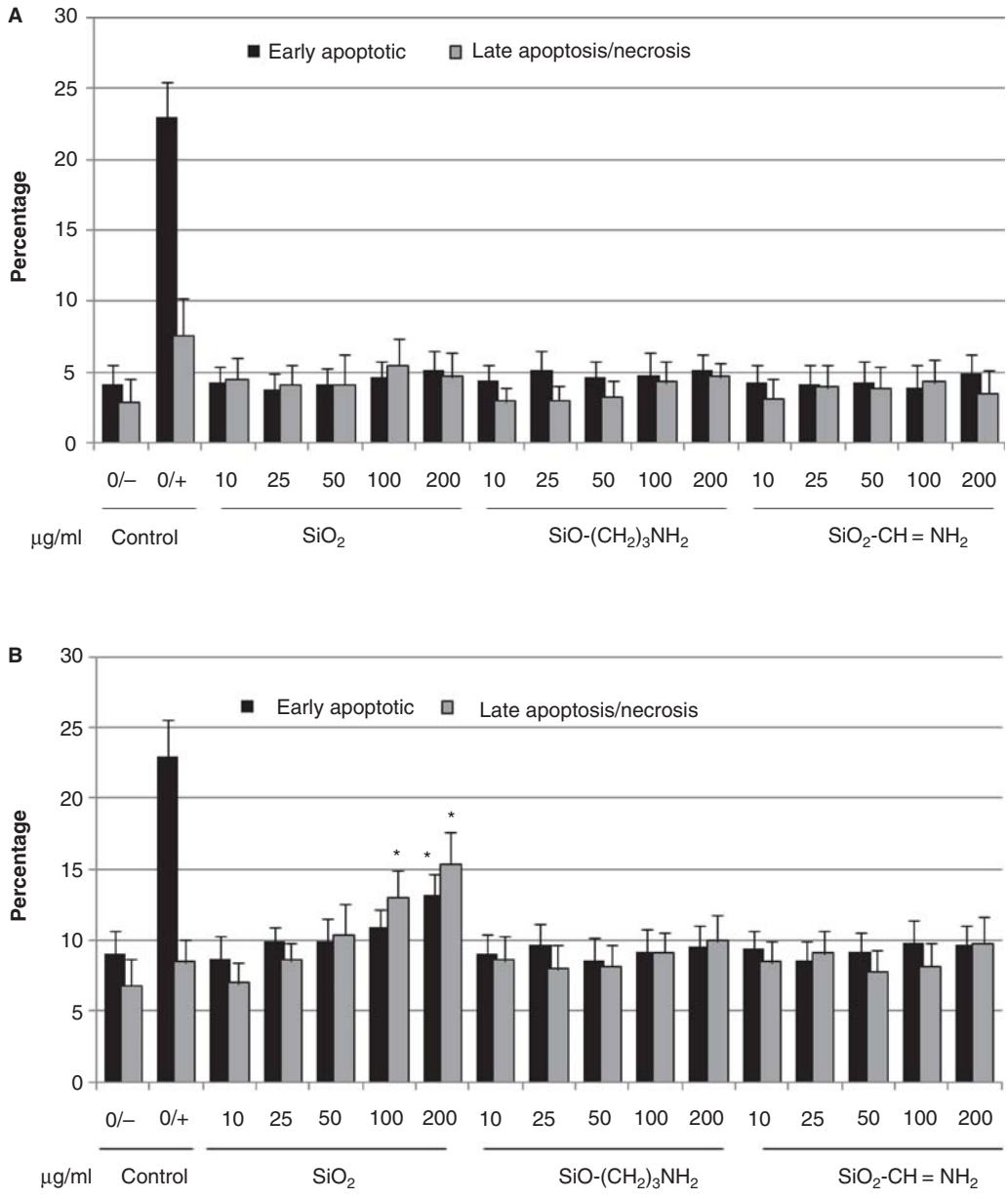

Figure 9. Flow cytometric analysis of apoptosis and necrosis in human peripheral blood lymphocytes *in vitro*, exposed to increasing doses of unmodified (SiO_2), vinyl-modified ($SiO\text{-}CH = CH_2$) and aminopropyl/vinyl-modified ($SiO\text{-}(CH_2)3NH_2$) silica nanoparticles for 2 and 24 h. (A) Frequency of apoptotic and necrotic cells exposed to 10, 25, 50, 100 and 200 μg/ml of silica nanoparticles for 2 h. (B) Frequency of apoptotic and necrotic cells exposed to 10, 25, 50, 100 and 200 μg/ml of silica nanoparticles for 24 h. Data are expressed as means ± S.D. from three independent experiments. Significant difference versus control, $^*p < 0.05$.

apoptotic/necrotic cells between untreated lymphocytes and lymphocytes treated with modified silica nanoparticles for 2 and 24 h. The frequency of early and late apoptotic/necrotic cells was markedly increased in lymphocytes treated with 100 and 200 μg/ml of unmodified silica nanoparticles for 24 h.

The effect of silica nanoparticles on DNA damage

The effect of different doses of unmodified and surface modified silica nanoparticles (10, 25, 50 and 100 ug/ml) on DNA damage was determined in human peripheral blood lymphocytes after 2 and 24 h. Comet assay results revealed no significant increase of basal DNA strand breaks (without Fpg digestion) in cells treated with all three types of silica nanoparticles after 2 and 24 h (Figure 10A, B). The level of oxidative base damage-derived DNA breaks (with Fpg digestion) was markedly increased in cells treated with 100 μg/ml of unmodified silica nanoparticles for 24 h.

The effect of silica nanoparticles on chromosome aberrations and mitotic indices

The frequency of chromosome aberrations was determined in human peripheral blood lymphocytes treated with 10, 25, 50 and 100 μg/ml of vinyl-modified, aminopropyl/vinyl-modified silica nanoparticles and unmodified silica nanoparticles for 50 h (approximate time of the first mitotic wave). As shown in Table IV, all three types of nanoparticles had no significant effect on the frequencies of chromosome

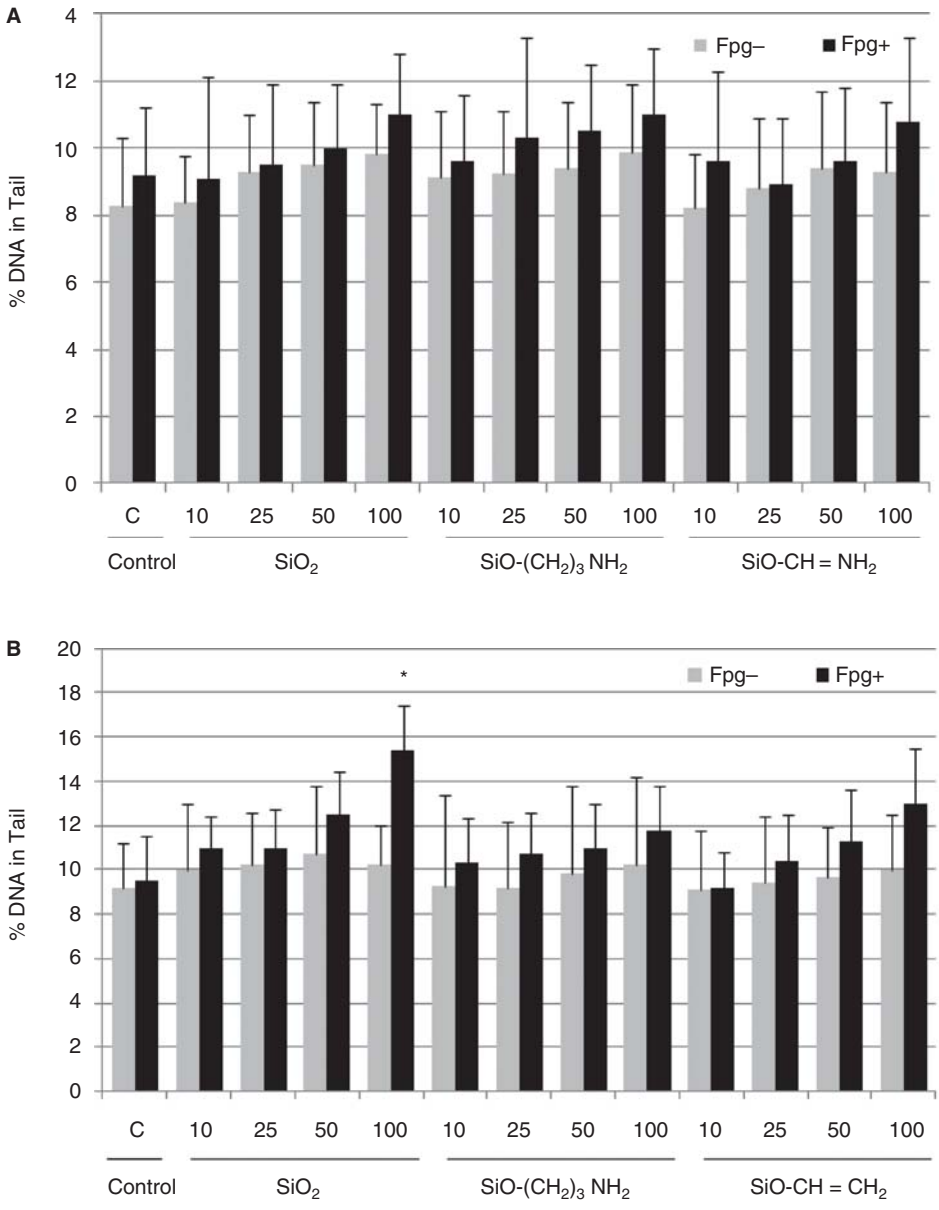

Figure 10. Effect of different doses of unmodified (SiO_2), vinyl-modified (SiO-CH = CH_2) and aminopropyl/vinyl-modified (SiO-$(CH_2)_3NH_2$) silica nanoparticles on the level of basal DNA damage without enzymatic digestion (gray bars) and oxidized purines with Fpg digestion (black bars) after 2 and 24 h. (A) DNA damage in human peripheral blood lymphocytes exposed to 10, 25, 50 and 100 μg/ml of silica nanoparticles for 2 h. (B) DNA damage in human peripheral blood lymphocytes exposed to 10, 25, 50 and 100 μg/ml of silica nanoparticles for 24 h. Data are expressed as means ± S.D. from three independent experiments. Significant difference versus control, *$p < 0.05$.

aberrations in lymphocytes. Increased frequency of aberrations per cell was found only in the positive control group exposed to 2 Gy of ionizing radiation (IR = 0.132 ± 0.021 vs. control = 0.015 ± 0.003). Mitotic indices were analyzed on the same slides that were used for estimation of chromosome aberrations. As shown in Table IV, exposure of human lymphocytes to increasing concentrations of silica nanoparticles resulted in dose-dependent changes in mitotic indices. Markedly decreased mitotic indices were found in lymphocytes treated with 25, 50 and 100 μg/ml of unmodified and modified silica nanoparticles.

Flow cytometric analysis of the cell cycle

The cell cycle in human peripheral blood lymphocytes was evaluated using the propidium iodide technique and flow cytometry (Figure 11). After stimulation of control lymphocytes with PHA for 50 h, there were 73.33% at G0/G1 phases and 26.67% at S/G2/M phases. As shown in Table V, all three types of nanoparticles inhibited the progression of cell cycles from G0/G1 phase to S/G2/M phases in a dose-dependent manner.

Discussion

The aim of the study was to synthesize and characterize the vinyl-modified and aminopropyl/vinyl-modified silica nanoparticles and to determine the cellular binding/uptake of these nanoparticles into human peripheral blood lymphocytes *in vitro* and the resulting biological response. These functional groups were chosen because of their potential for

Table IV. The frequencies of chromosome aberrations and mitotic indices in human peripheral blood lymphocytes treated with silica nanoparticles (10, 25, 50, 100 μg/ml) for 50 h.

		mitotic index (1000)	Aberrations per cell
Experimental group	Treatment	Mean ± SD	Mean ± SD
Negative control	0	6,34 ± 1,3	0,015 ± 0,003
Positive control	2 Gy	4,12 ± 1,2	0,132 ± 0,021*
Unmodified silica nanoparticles	10 μg/ml	5,12 ± 0,9	0,014 ± 0,002
	25 μg/ml	3,54 ± 1,3*	0,015 ± 0,001
	50 μg/ml	2,75 ± 0,6*	0,015 ± 0,002
	100 μg/ml	1,62 ± 0,5*	0,018 ± 0,002
Vinyl-modified silica nanoparticles	10 μg/ml	5,78 ± 1,0	0,012 ± 0,003
	25 μg/ml	4,23 ± 0,9*	0,017 ± 0,001
	50 μg/ml	3,51 ± 0,7*	0,011 ± 0,002
	100 μg/ml	2,76 ± 0,9*	0,016 ± 0,002
Aminopropyl/ vinyl-modified silica nanoparticles	10 μg/ml	5,92 ± 0,9	0,016 ± 0,003
	25 μg/ml	4,38 ± 1,1	0,016 ± 0,001
	50 μg/ml	3,67 ± 0,8*	0,014 ± 0,002
	100 μg/ml	2,52 ± 0,8*	0,018 ± 0,001

Numbers in brackets show the numbers of analyzed cells per point. Pooled data from three independent experiments with the standard deviations of the means are given; *Difference to control significant with $p < 0.05$.

subsequent bioconjugation and biomedical applications (Bagwe et al. 2006). In addition, we tested unmodified silica nanoparticles to evaluate whether surface functionalization alters the biological properties of silica nanoparticles.

Our study demonstrated that a water suspension sol-gel process and the Stöber method allowed to obtain with high yield the amorphous vinyl-modified and aminopropyl/vinyl-modified silica nanoparticles of spherical shape and uniform size in the range of 10–50 nm. These particles exhibited the average surface area in the range of 250–350 m^2/g with pore volume of 0.64–1.13 cm^3/g. The unmodified silica nanoparticles were spherical and porous with diameter in the range of 10–50 nm and average surface area in the range of 590–690 m^2/g.

To determine the kinetics of cellular uptake of the studied nanoparticles into human peripheral blood lymphocytes we used flow cytometry. The SSC distribution ratio was chosen as a measure of cellular binding/uptake according to Suzuki et al. (2007) and Zucker et al. (2010). Our results revealed that the uptake of all three types of nanoparticles was dose- and time-dependent. The cellular binding/uptake increased gradually and reached a plateau after 12–14 h, depending on the type of nanoparticles. These results are in line with the data presented by Stayton et al. (2009), who observed that the number of silica nanoparticles increased linearly in A549 cells up to 8–10 h and reached saturation. Shapero et al. (2011) monitored the uptake of uncoated fluorescent labeled silica nanoparticles of different sizes into A549 cells and found that the uptake is higher for the smaller nanoparticle sizes. Interestingly, our results have shown (Figure 7) that the efficiency of cellular binding/uptake is also dependent on surface modification. The uptake of aminopropyl/vinyl-modified silica nanoparticles by lymphocytes was more efficient than that of vinyl-modified and unmodified silica nanoparticles.

A significant body of recent literature documents that particle size, shape and surface functionality, in particular surface charge and zeta-potential, affect the interactions between particles and cells (Barbosa et al. 2007; Thevenot et al. 2008). Different efficiencies of cellular binding/uptake of the same size and shape silica nanoparticles observed in our study suggest that in this case other factors, for example, modification of surface charge and zeta-potential, are important. The zeta potential determined at 1.63×10^{-1} mol/kg in cell culture medium pH 7.4 was equal +18.16 mV for the aminopropyl/vinyl-modified silica nanoparticles, −9.49 mV for the vinyl modified silica nanoparticles and -13.32 mV for the unmodified silica nanoparticles. These results indicate that nanoparticles with positive zeta potential may facilitate the cellular binding/uptake of nanoparticles. Our findings are in agreement with Stayton et al. (2009), who showed that histone-coated silica nanoparticles with the least negative zeta-potential had been taken up into A549 cells more efficient than other nanoparticles tested. Qiu et al. (2010) reported that a positive surface charge facilitated this process. Positively charged functional groups, particularly amine groups, have been shown to engage in strong ionic interaction with the negatively charged cell membrane, which favors cell attachment and uptake (Wilson et al. 2005). In contrast, Chung et al. (2007) demonstrated that a strongly positive surface charge inhibited the uptake. The relationship between the surface charge and the efficiency of cellular uptake of nanoparticles was also presented by others (Foged et al. 2005; Lee et al. 2006; Chung et al. 2007), but these reports provide inconsistent information about dependency of cellular uptake of nanoparticles on their surface charge and zeta-potential.

Due to the potential use of the aminopropyl and vinyl-modified silica nanoparticles in biomedical applications, it is crucial to investigate their biocompatibility. In the present study we used human peripheral blood lymphocytes as an experimental *in vitro* model because they circulate in the whole organism, pass back and forth between blood, lymph tissue, lymph fluid and all tissues. Moreover, they are critical to body defense (Rajakariar et al. 2008). The overall results of the cytotoxicity studies showed that the frequencies of viable, early apoptotic and late apoptotic/necrotic cells were not affected by surface-modified silica nanoparticles. In contrast, the flow cytometric analysis showed that unmodified silica nanoparticles produced cytotoxic effect to lymphocytes *in vitro* at the high doses. These nanoparticles at concentrations of 100 and 200 μg/ml decreased significantly the frequency of viable cells after 24 h of treatment. The decreased viability was associated with the increased frequency of late apoptotic/necrotic cells. These results are in agreement with many recently published results indicating that unmodified amorphous silica nanoparticles induce cytotoxicity in several cell lines at concentrations >50 μg/ml (Barnes et al. 2008; Yu et al. 2009; Kim et al. 2009; Nabeshi et al. 2010; Liu & Sun 2010). Based on our data, it seems that functionalization of silica nanoparticles by the vinyl and aminopropyl groups may inhibit their cytotoxic properties. This suggestion is in line with the results obtained by Di Pasqua et al. (2008), who revealed that the mesoporous aminopropyl/vinyl-modified silica nanoparticles were less toxic than the unmodified analogue.

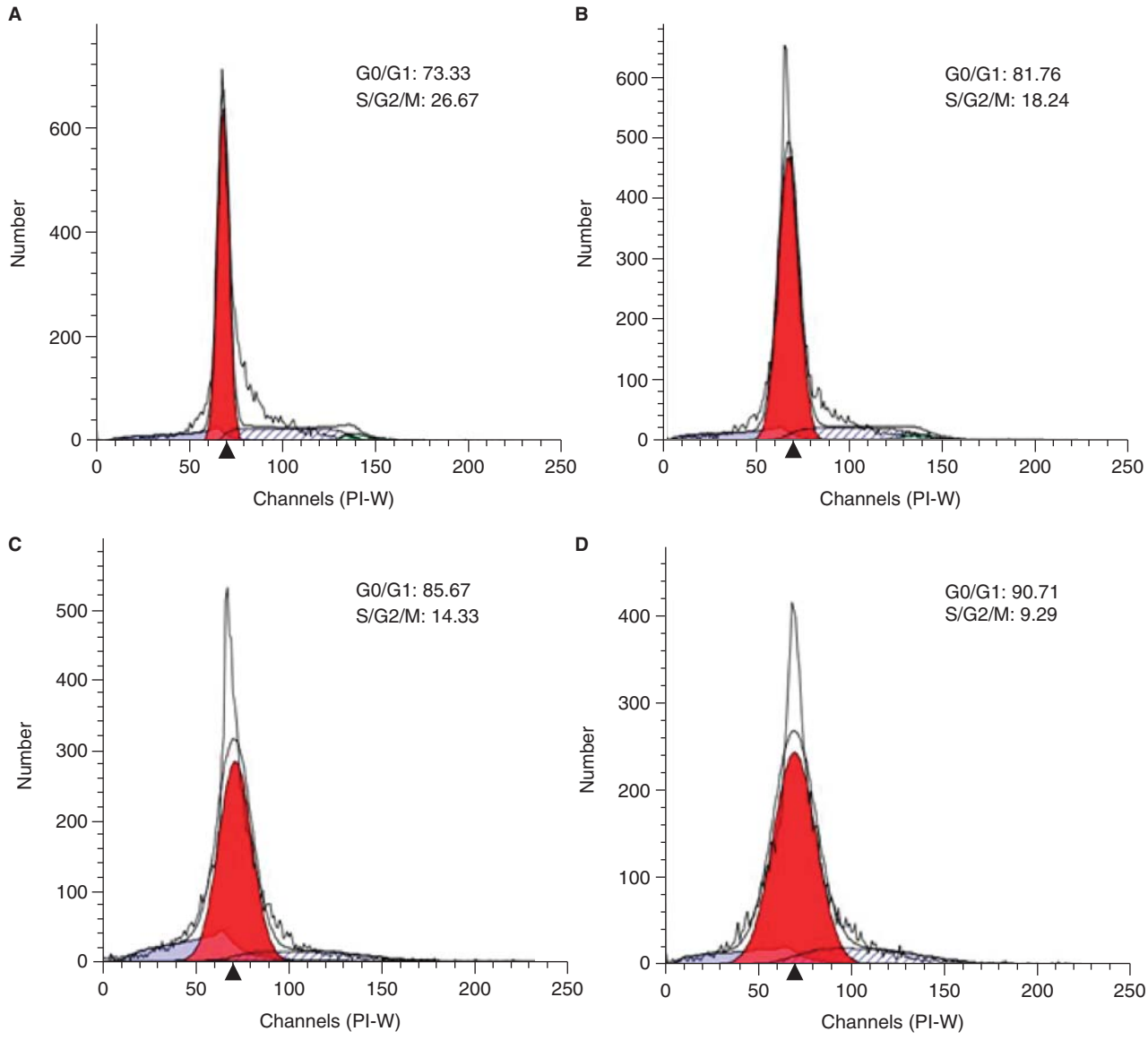

Figure 11. Cell cycle analysis of PHA-stimulated human peripheral blood lymphocytes treated with silica nanoparticles for 50 h. The graphs are representative of the three independent experiments, each showing similar results. (A) control cells; (B) cells treated with 25 μg/ml of aminopropyl/vinyl-modified silica nanoparticles; (C) cells treated with 50 μg/ml of aminopropyl/vinyl-modified silica nanoparticles; (D) cells treated with 100 μg/ml of aminopropyl/vinyl-modified silica nanoparticles. G0/G1 phases (one set of paired chromosomes per cell), S/G2/M phases (DNA synthesis with variable amount of DNA and two sets of paired chromosomes per cell).

Similar findings, indicating that functional groups grafted on nanoparticles alter their toxicity, were published by others (Barnes et al. 2008; Thevenot et al. 2008; Slowing et al. 2009).

However, a question arises regarding the reasons of the observed difference in toxicity between unmodified and modified silica nanoparticles. There appear to be two possible explanations. Firstly, the reduced cell viability could result from higher surface area of the unmodified silica nanoparticles than that of the aminopropyl/vinyl-modified as well as the vinyl-modified ones (BET = 640 m2/g vs. BET = 260 m^2/g and BET = 350 m^2/g, respectively.) It was shown by Oberdörster et al. (2005) that the cellular response is proportional to particle BET surface area. Similar results were published by Teeguarden et al. (2007) and Di Pasqua et al. (2008). However, recent report by Maurer-Jones et al. (2010) shows that cell contactable surface area might be more important for nanoparticle property than total surface area in regards to cellular uptake.

The second factor responsible for the reduced cell viability could be due to the more efficient induction of reactive oxygen species (ROS) by unmodified silica nanoparticles than by the surface-modified ones. Recently, it was reported that treatment of RAW264.7 cells in culture with amorphous silica nanoparticles led to ROS generation accompanied by a decreased intracellular glutathione (Park & Park 2009). Similar results were published by Ye et al. (2010) who observed an increased production of ROS in myocardial H9c2(2-1) cells exposed to amorphous silica nanoparticles with sizes of 21 and 48 nm. Moreover, ROS production and oxidative stress have been reported as the toxic mechanism of silica nanoparticle-induced apoptosis and necrosis in various cell types (Eom & Choi et al. 2009; Choi et al. 2009; Liu & Sun

Table V. Cell cycle analysis of PHA stimulated human peripheral blood lymphocytes treated with silica nanoparticles (25, 50, 100 μg/ml) for 50 h.

Experimental group	Treatment	G0/G1 [%] Mean ± SD	S/G2/M [%] Mean ± SD
Control	0	73.33 ± 2.62	26.67 ± 2,13
Unmodified silica nanoparticles	25 μg/ml	82.46 ± 1.33*	17.54 ± 2.14*
	50 μg/ml	86.67 ± 2.56*	13.33 ± 1.57*
	100 μg/ml	91.58 ± 3.15*	8.42 ± 1.32*
Vinyl-modified silica nanoparticles	25 μg/ml	80.79 ± 2.71*	19.21 ± 2.73*
	50 μg/ml	85.36 ± 3.11*	14.64 ± 2.11*
	100 μg/ml	89.88 ± 1.98*	10.12 ± 1.45*
Aminopropyl/ vinyl-modified silica nanoparticles	25 μg/ml	81.76 ± 2.24*	18.24 ± 2.43*
	50 μg/ml	85.67 ± 3.24*	14.33 ± 1.98*
	100 μg/ml	90.71 ± 4.13*	9.29 ± 2.03*

Pooled data from three independent experiments with the standard deviations of the means are given; *Difference to control significant with $p < 0.05$.

2010). The efficiency of ROS production by the modified silica nanoparticles used in this study has not been explored yet. Hence, the role of ROS generation must be confirmed by further experiments.

To assess genotoxic properties of silica nanoparticles we used the modified comet assay (single cell gel electrophoresis) in conjunction with Fpg. This assay is able to detect basal DNA damage such as single and double strand breaks and alkali-labile lesions as well as oxidized purines (Hartmann et al. 2004; Collins et al. 1993). The results of our study revealed no significant increase of basal DNA strand breaks (without Fpg digestion) in lymphocytes treated with all three types of silica nanoparticles for 2 and 24 h. Our results are in line with Barnes et al. (2008), who found in the comet assay that commercial colloidal and laboratory-synthesized silica nanoparticles (20–400 nm) cause no significant increase of basal DNA damage. The level of oxidative base damage-derived DNA breaks (with Fpg digestion) was significantly increased only in cells treated with the unmodified silica nanoparticles, as compared to the untreated control group. These data suggest that functionalization of silica nanoparticles by vinyl and aminopropyl groups may inhibit their genotoxic properties. Recently, Shi et al. (2010) applied the modified comet assay to A549 cells and also observed a low effect of silica nanoparticles on oxidative DNA damage. Similar results were documented by Yang et al. (2009) and Guidi et al. (2010), who showed in the comet assay that amorphous silica nanoparticles affected DNA integrity in primary mouse embryo fibroblast cells, but clear dose-effect relationship was not detected.

Since the enhanced level of oxidative base damage-derived DNA strand breaks may lead to chromosome rearrangements, we investigated whether silica nanoparticles can induce chromosome aberrations in human lymphocytes *in vitro*. Our results revealed that all three types of silica nanoparticles had no effect on the frequencies of chromosome aberrations. Similar results were published by Gonzalez et al. (2010), who observed a weak but not statistically significant induction of chromosome breakage and chromosome loss in A549 cells exposed to silica nanoparticles. In contrast, Park et al. (2010) found that silica nanoparticles induced chromosomal aberrations in 3T3-L1 mouse fibroblasts and gene mutations in mouse embryonic fibroblasts carrying the lacZ reporter gene.

We suppose that the lack of correlation between the results of chromosome and comet assays may be due to the fact that the tolerable doses of silica nanoparticles were efficient enough to induce oxidative DNA damage, followed by single strand breaks formed during DNA repair, but were too low to induce double strand breaks that may lead to chromosome aberrations. This presumption is consistent with the finding of Rueff et al. (1993) who observed that DNA single-strand breaks produced by low doses of ionizing radiation and H2O2 are not abundant enough to induce chromosome aberrations. Apart from chromosome aberrations, we also measured mitotic indices in lymphocytes treated for 50 h with silica nanoparticles to examine their impact on the proliferation status. Interestingly, we found that exposure of human lymphocytes to increasing concentrations of all three types of silica nanoparticles resulted in a dose-dependent decrease in the mitotic index values. To our knowledge, the proliferation status in lymphocytes exposed to silica nanoparticles has never been documented. However, a few papers reported the reduced mitotic index values in cells exposed to silver, chitosan and titanium dioxide nanoparticles (Kumari et al. 2009; Lima et al. 2010; Klančnik et al. 2011). To confirm our assumption that silica nanoparticles might be involved in cell cycle progression resulting in a dose-dependent decrease in the mitotic index values, we analyzed the cell cycle in human peripheral blood lymphocytes treated with unmodified and modified silica nanoparticles for 50 h. Our results clearly revealed that all three types of silica nanoparticles inhibited the progression of cell cycle from G1 to S phases in a dose-dependent manner. Since we do not know the nature of the blocked state, we can't give an unequivocal conclusion whether this state will lead to cytotoxic effect such as apoptosis, senescence of these cells or that this state will be reversible. It was found by Borel et al. (2002) that mammalian cells arrested for a prolonged period of time at the G1/S boundary by drugs that interfere with initiation of DNA replication become permanently arrested. Depending on cell type (differentiated vs. undifferentiated), permanently arrested cells may be transformed into long-lived senescent cells or may be removed by apoptosis (Ben-Porath & Weinberg 2004). On the other hand, Lohez et al. (2003) reported that the progression of cell cycle can be inhibited by drugs that interfere with cytoskeleton proteins, but this state is reversible.

In summary, we synthesized and characterized the vinyl-modified and aminopropyl/vinyl-modified silica nanoparticles, which were amorphous and mesoporous and had spherical shape and uniform size. Biocompatibility studies indicated that the vinyl-modified and aminopropyl/vinyl-modified silica nanoparticles were internalized by human lymphocytes with varying efficiency levels. These nanoparticles exhibited no significant cytotoxic and genotoxic properties under experimental conditions. However, they affected the proliferation of the lymphocyte population as showed

by the decreased values of mitotic indices and inhibited progression of cells from G1 to S phases of cell cycle. In contrast, unmodified silica nanoparticles exerted cytotoxic and genotoxic properties at high doses by increasing apoptosis and oxidative DNA damage as well as inhibited the progression of cell cycle from G1 to S phases. Further experiments dealing with spindle formation and cell division are needed to evaluate how the vinyl-modified and aminopropyl/vinyl-modified silica nanoparticles disturb the cell cycle progression.

Acknowledgements

This study was supported by the Ministry of Science and Higher Education, Poland, grant number N N401 191836. The authors thank Adam Presz from the Institute of High Pressure Physics, Polish Academy of Sciences, for assistance with scanning electron microscopy. The authors also acknowledge the assistance of Monica Borrin-Flint in the preparation of the manuscript.

Declaration of interest

The authors report no conflicts of interest. The authors alone are responsible for the content and writing of the paper.

References

An Y, Chen M, Xue Q, Liu W. 2007. Preparation and self-assembly of carboxylic acid-functionalized silica. J Colloid Interface Sci 311:507–513.

Arkhireeva A, Hay JN. 2003. Synthesis of sub-200 nm silsesquioxane particles using a modified Stöber sol–gel route. J Mater Chem 13:3122.

Bagwe RP, Hilliard L, Tan W. 2006. Surface modification of silica nanoparticles to reduce aggregation and nonspecific binding. Langmuir 22:4357–4362.

Barbosa EM, Montembault V, Cammas-Marion S, Ponchel G, Fontaine L. 2007. Synthesis and characterization of novel poly (γ-benzyl-L-glutamate) derivatives tailored for the preparation of nanoparticles of pharmaceutical interest. Polym Int 56:317–324.

Barik TK, Sahu B, Swain V. 2008. Nanosilica-from medicine to pest control. Parasitol Res 103:253–258.

Barnes CA, Elsaesser A, Arkusz J, Smok A, Palus J, Leśniak A, et al. 2008. Reproducible comet assay of amorphous silica nanoparticles detects no genotoxicity. Nano Lett 8:3069–3074.

Ben-Porath I, Weinberg RA. 2004. When cells get stressed: an integrative view of cellular senescence. J Clin Invest 113:8–13.

Borel F, Lacroix FB, Margolis RL. 2002. Prolonged arrest of mammalian cells at the G1/S boundary results in permanent S phase stasis. J Cell Sci 115:2829–2838.

Cho YS, Yoon TJ, Jang ES, Soo Hong K, Young Lee S, Ran Kim O, et al. 2010. Cetuximab-conjugated magneto-fluorescent silica nanoparticles for in vivo colon cancer targeting and imaging. Cancer Lett; [Epub ahead of print].

Choi SJ, Oh JM, Choy JH. 2009. Toxicological effects of inorganic nanoparticles on human lung cancer A549 cells. J Inorg Biochem 103:463–471.

Chung T-H, Wu S-H, Yao M, Lu C-W, Lin Y-S, Hung Y, et al. 2007. The effect of surface charge on the uptake and biological function of mesoporous silica nanoparticles in 3T3-L1 cells and human mesenchymal stem cells. Biomaterials 28:2959–2966.

Collins AR, Duthie SJ, Dobson VL. 1993. Direct enzymatic detection of endogenous oxidative base damage in human lymphocyte DNA. Carcinogenesis 14:1733–1735.

Collins AR. 2004. Comet Assay for DNA damage and repair: principles, applications and limitations. Mol Biotechnol 26:249–261.

Darzynkiewicz Z. 2003. Current protocols in Cell Biology. John Wiley & Sons, Inc. New York.

De Lima R, Feitosa L, Pereira AE, De Moura MR, Aouada FA, Mattoso LH, et al. 2010. Evaluation of the genotoxicity of chitosan nanoparticles for use in food packaging films. J Food Sci 75:N89–N96.

Di Pasqua AJ, Sharma KK, Shi Y-L, Toms BB, Ouellette Dabrowiak JC, Asefa T. 2008. Cytotoxicity of mesoporous silica nanomaterials. J Inorg Biochem 102:1416–1423.

Di Pasqua L, Testa F, Aiello R, Cundari S, Nagy JB. 2007. Preparation of bifunctional hybrid mesoporous silica potentially useful for drug targeting. Micropor Mesopor Mater 103:166–173.

Eom HJ, Choi J. 2009. Oxidative stress of silica nanoparticles in human bronchial epithelial cell, Beas-2B. Toxicol In Vitro 23:1326–1332.

Foged C, Brodin B, Frokjaer S, Sundblad A. 2005. Particle size and surface charge affect particle uptake by human dendritic cells in an in vitro model. Int J Pharm 298:315–322.

Gonzalez L, Thomassen LC, Plas G, Rabolli V, Napierska D, Decordier I, et al. 2010. Exploring the aneugenic and clastogenic potential in the nanosize range: A549 human lung carcinoma cells and amorphous monodisperse silica nanoparticles as models. Nanotoxicology 4:382–395.

Green DL, Lin JS, Lam Y-F, Dale H, Schaefer W, Harris MT. 2003. Size, volume fraction, and nucleation of Stober silica nanoparticles. J Colloid Interface Sci 266:346–358.

Guidi P, Scarcelli V, Bernardeschi M, Lucchesi P, Nigro M, Frenzilli G. 2010. Potential genotoxic effects induced by different superficial morphologies and different dimensions of amorphous silica powders evaluated in murine alveolar macrophages (Raw 264.7) cell lines. Comp Biochem Physiol A 157: S12–S14.

Hartmann A, Schumacher M, Plappert-Helbig U, Lowe P, Suter W, Mueller L. 2004. Use of the alkaline in vivo Comet assay for mechanistic genotoxicity investigations. Mutagenesis 19:51–59.

Holmes PF, Currie EP, Thies JC, van der Mei HC, Busscher HJ, Norde W. 2009. Surface-modified nanoparticles as a new, versatile, and mechanically robust nonadhesive coating: suppression of protein adsorption and bacterial adhesion. J. Biomed Mater Res A 91:824–833.

Hom C, Lu J, Tamanoi F. 2009. Silica nanoparticles as a delivery system for nucleic acid-based reagents. J Mater Chem 19:6308.

Kim HW, Ahn EK, Jee BK, Yoon H-K, Lee KH, Lim Y. 2009. Nanoparticulate-induced toxicity and related mechanism *in vitro* and *in vivo*. J Nanoparticle Res 11:55–65.

Klančnik K, Drobne D, Valant J, Koce JD. 2011. Use of a modified Allium test with nanoTiO_2. Ecotoxicol Environ Saf 74:85–92.

Knopp D, Tang D, Niessner R. 2009. Review: bioanalytical applications of biomolecule-functionalized nanometer-sized doped silica particles. Anal Chim Acta 647:14–30.

Krishan A. 1975. Rapid flow cytofluorometric analysis of mammalian cell cycle by propidium iodide staining. J Cell Biol 66:188–193.

Kruszewski M, Wojewódzka M, Iwaneńko T, Collins AR, Szumiel I. 1998. Application of the comet assay for monitoring DNA damage in workers exposed to chronic low dose irradiation. II. Base damage. Mutat Res 416:37–57.

Kumari M, Mukherjee A, Chandrasekaran N. 2009. Genotoxicity of silver nanoparticles in Allium cepa. Sci Total Environ 407:5243–5246.

Lankoff A, Banasik A, Obe G, Deperas M, Kuźmiński K, Tarczyńska M, et al. 2003. Effect of microcystin-LR and cyanobacterial extract from Polish reservoir of drinking water on cell cycle progression, mitotic spindle and apoptosis in CHO-K1 cells. Toxicol Appl Pharmacol 189:204–213.

Lee D, Kim J-W, Kim BG. 2006. A new parameter to control heat transport in nanofluids: surface charge state of the particle in suspension. J Phys Chem B 110:4323–4328.

Liu X, Sun J. 2010. Endothelial cells dysfunction induced by silica nanoparticles through oxidative stress via JNK/P53 and NF-kappaB pathways. Biomaterials 31:8198–8209.

Lohez OD, Reynaud C, Borel F, Andreassen PR, Margolis RL. 2003. Arrest of mammalian fibroblasts in G1 in response to actin inhibition is dependent on retinoblastoma pocket proteins but not on p53. J Cell Biol 161:67–77.

Maurer-Jones MA, Lin Y-S, Chynes CL. 2010. Functional assessment of metal oxide nanoparticle toxicity in immune cells. ASC Nano 4:3363–3373.

Nabeshi H, Yoshikawa T, Matsuyama K, Nakazato Y, Arimori A, Isobe M, et al. 2010. Size-dependent cytotoxic effects of amorphous silica nanoparticles on Langerhans cells. Pharmazie 65:199–201.

Oberdörster G, Maynard A, Donaldson K, Castranova V, Fitzpatrick J, Ausman K, et al. 2005. Principles for characterizing the potential human health effects from exposure to nanomaterials: elements of a screening strategy. ILSI Research Foundation/Risk Science Institute Nanomaterial Toxicity Screening Working Group. Part Fibre Toxicol 6:2–8.

Park EJ, Park K. 2009. Oxidative stress and pro-inflammatory responses induced by silica nanoparticles in vivo and in vitro. Toxicol Lett 184:18–25.

Park MV, Verharen HW, Zwart E, Hernandez LG, van Benthem J, Elsaesser A, et al. 2010. Genotoxicity evaluation of amorphous silica nanoparticles of different sizes using the micronucleus and the plasmid lacZ gene mutation assay. Nanotoxicology; Epub ahead of print.

Perrin DD, Armarego WLF, Perrin DR. 1980. In Purification of Laboratory Chemicals. New York: Pergamon Press.

Perry P, Wolff S. 1974. New Giemsa method for the differential staining of sister chromatids. Nature 251:156–158.

Qiu J, Liu Y, Wang L, Xu L, Bai R, Ji Y, Wu X, Zhao Y, Li Y, Chen C. 2010. Surface chemistry and aspect ratio mediated cellular uptake of Au nanorods. Biomaterials 31:7606–7619.

Rajakariar R, Lawrence T, Bystrom J, Hilliard M, Colville-Nash P, Bellingan B, et al. 2008. Novel biphasic role for lymphocytes revealed during resolving. Blood 111:4184–4192.

Rosenholm JM, Sahlgren C, Lindén M. 2010. Towards multifunctional, targeted drug delivery systems using mesoporous silica nanoparticles - opportunities and challenges. Nanoscale; [Epub ahead of print].

Rózga-Wijas K, Chojnowski J, Ścibiorek M, Fortuniak W. 2005. Polysiloxane-silica hybrids from novel precursors by the sol-gel process. J Mater Chem 15:2383–2392.

Rueff J, Bras A, Cristovao L, Mexia J, Sa da Costa M, Pires V. 1993. DNA strand breaks and chromosomal aberrations induced by H_2O_2 and 60Co gamma-radiation. Mutat Res 289:197–204.

Savage JRK. 1975. Classification and relationships of induced chromosomal structural changes. J Med Genet 12:103–122.

Shapero K, Fenaroli F, Lynch I, Cottell DC, Salvati A, Dawson KA. 2011. Time and space resolved uptake study of silica nanoparticles by human cells. Mol BioSyst 7:371–378.

Shi Y, Yadav S, Wang F, Wang H. 2010. Endotoxin promotes adverse effects of amorphous silica nanoparticles on lung epithelial cells in vitro. J Toxicol Environ Health A 73:748–756.

Slowing II, Wu C-W, Vivero-Escoto JL, Lin VS-Y. 2009. Mesoporous silica nanoparticles for reducing hemolytic activity towards mammalian red blood cells. Small 5:57–62.

Stayton I, Winiarz J, Shannon K, Ma Y. 2009. Study of uptake and loss of silica nanoparticles in living human lung epithelial cells at single cell level. Anal Bioanal Chem 394:1595–1608.

Stöber W, Fink A. 1968. Controlled growth of mono- disperse silica spheres in the micron size range. J Colloid Interface Sci 26:62.

Suzuki H, Toyooka T, Ibuki Y. 2007. Simple and easy method to evaluate uptake potential of nanoparticles in mammalian cells using a flow cytometric light scatter analysis. Environ Sci Technol 41:3018–3024.

Taylor KM, Kim JS, Rieter WJ, An H, Lin W, Lin W. 2008. Mesoporous silica nanospheres as highly efficient MRI contrast agents. J Am Chem Soc 130:2154–2155.

Teeguarden JG, Hinderliter PM, Orr G, Thrall BD, Pounds JG. 2007. Particokinetics in vitro: dosimetry considerations for in vitro nanoparticle toxicity assessments. Toxicol Sci 95:300–312.

Thevenot P, Cho J, Wavhal D, Timmons RB, Tang L. 2008. Surface chemistry influences cancer killing effect of TiO_2 nanoparticles. Nanomedicine 4:226–236.

Vallet-Regí M, Balas F, Arcos D. 2007. Mesoporous materials for drug delivery. Angew Chem Int Ed Engl 46:7548–7558.

Wilson CJ, Clegg RE, Leavesley DI, Pearcy MJ. 2005. Mediation of biomaterial-cell interactions by adsorbed proteins: a review. Tissue Eng 11:1–18.

Wojewódzka M, Kruszewski M, Iwaneńko T, Collins AR, Szumiel I. 1998. Application of the comet assay for monitoring DNA damage in workers exposed to chronic low dose irradiation. I. Strand breakage. Mutat Res 416:21–35.

Yang H, Liu C, Yang D, Zhang H, Xi Z. 2009. Comparative study of cytotoxicity, oxidative stress and genotoxicity induced by four typical nanomaterials: the role of particle size, shape and composition. J Appl Toxicol 29:69–78.

Ye Y, Liu J, Xu J, Sun L, Chen M, Lan M. 2010. Nano-SiO_2 induces apoptosis via activation of p53 and Bax mediated by oxidative stress in human hepatic cell line. Toxicol In Vitro 24:751–758.

Yu KO, Grabinski CM, Schrand AM, Murdock RC, Wang W, Gu B, et al. 2009. Toxicity of amorphous silica nanoparticles in mouse keratinocytes. J Nanoparticle Res 11:15–24.

Zucker RM, Massaro EJ, Sanders KM, Degn LL, Boyes WK. 2010. Detection of TiO_2 nanoparticles in cells by flow cytometry. Cytometry Part A 77A:677–685.

Supplementary material available online

Supplementary Tables SI, SII.
Supplementary Figures S1, S2.